doi:10.1038/nature13499

A deep crust–mantle boundary in the asteroid 4 Vesta

Harold Clenet[1], Martin Jutzi[2], Jean-Alix Barrat[3], Erik I. Asphaug[4], Willy Benz[2] & Philippe Gillet[1]

The asteroid 4 Vesta was recently found to have two large impact craters near its south pole, exposing subsurface material. Modelling suggested that surface material in the northern hemisphere of Vesta came from a depth of about 20 kilometres, whereas the exposed southern material comes from a depth of 60 to 100 kilometres. Large amounts of olivine from the mantle were not seen, suggesting that the outer 100 kilometres or so is mainly igneous crust. Here we analyse the data on Vesta and conclude that the crust–mantle boundary (or Moho) is deeper than 80 kilometres.

Global mapping with high-resolution imagery by the Dawn probe revealed that the south polar depression is composed of two overlapping impact basins, Veneneia and Rheasilvia[1]. This discovery is critical in the search for the Mohorovičić discontinuity (Moho). Indeed, although a single impact is expected to excavate rocks only from the crust, recent numerical simulations[2,3] taking into account both sequential events show that excavation and ejection of mantle material during the second impact would be facilitated because the first one would have already thinned or removed the crust locally.

Impact simulations in three dimensions have been able to reproduce Vesta's topography accurately[2]. The results of this model allow the source depths or provenances of rocks to be directly investigated today. Two distinct sets of observables are considered for comparison with modelling observations: the surface of Vesta, which includes the material outcropping in the basins and the ejecta covering the rest of the asteroid, and the meteoroids and asteroids that escaped during the impacts and are the probable source of the howardite–eucrite–diogenite (HED) meteorites originating from Vesta[4].

Mapping the predicted provenance of surface material (Fig. 1) shows that a large amount of the rocks exposed in the south pole region should come from depths exceeding 50 km. Simulations predict initial depths of up to ~60–100 km in the central mound of Rheasilvia and in the region where the impact basins overlap[2]. If the crust of Vesta is ~30–40 km thick, as proposed in magma-ocean crystallization models[5–8], a succession of two impacts would have dug well into the mantle, producing large outcrops of olivine-rich rocks within the basins.

Mineralogical mapping of Vesta's surface with images from the VIR instrument onboard the Dawn probe shows that pyroxenes are ubiquitous in the southern hemisphere, while no olivine is observed[9–11], even where rocks come from the deepest levels in numerical simulations (Fig. 1). Admittedly, the mantle spectral signature could have been partially masked by late-impact gardening. But because the mantle is highly enriched in olivine, and because the outcrops occur over a broad expanse, some pixels should exhibit a definitive olivine signature. The conclusion that olivine does not represent a large mineral fraction of the rocks[12] is at odds with the higher content expected in deep mantle rocks, and argues against the idea that mantle is excavated and exposed by the successive impacts.

The HED meteorites[13] are a large collection of basaltic and ultramafic samples that originated from Vesta. There is no reason, a priori, why their relative proportions should equal the proportions of Vesta's surface covered by the different lithologies[13]. They come from the small asteroids (vestoids) that were ejected by the large impacts[14], so their proportions will, if anything, be representative of the lithologies that escaped Vesta. The amount of material escaping Vesta following both collisions can be reliably estimated[2] (see Methods). The first impact ejected away material from up to about 25 km deep (Fig. 2). The second overlapping impact dug deeper, up to 20–80 km below the original surface, because Rheasilvia formed on top of rocks excavated by Veneneia. A third of all the escaping material comes from depths greater than 40 km. So, if the assumption of a thin crust[7,8] is considered, samples of mantle should be found in the HED suite.

While the details of the mass distribution shown in Fig. 2 depend on the impact geometry, the overall result is robust because it is closely tied to the impact suite (model results) that best explains the detailed shape of Vesta. In addition, two distinct small asteroid populations are predicted, one for each of the massive cratering events, which is consistent with recent evidence for spectral colour variations within the Vesta family[15]. However, it is not clear to what degree the original proportions of the escaping materials have been changed during the dynamical and collisional evolution of the fragments. The total amount of material escaping Vesta as a result of the two giant impacts is approximately 2.7×10^{18} kg, according to smooth particle hydrodynamics (SPH) modelling[2], which is consistent with geological estimates of basin formation[1]. This exceeds the observational estimates of the total mass of the vestoids ($0.5–3 \times 10^{17}$ kg[3]). While these estimates do depend on the assumed size distribution[3], this does not change the fact that far more material escaped Vesta than is observed today.

This implies that the vestoids have been greatly eroded, as was already predicted by detailed simulations of the dynamical evolution of the Vesta family[16]. But there is no reason why this depletion would deplete the olivines—in escaping fragments of the deep mantle—and not the pyroxenes. If Vesta's mantle was originally about 40 km deep, then a third of the material escaping Vesta should have olivine-rich lithologies (see Fig. 2), and a significant fraction of the HEDs should come from deeper still. Olivine should be reflected in the composition of the main-belt and near-Earth vestoids as well as in the HED meteorite suite.

Only a few meteorites enriched in olivine have been collected, and they do not originate from the mantle, but instead formed in plutons[17]. One explanation for the 'missing' olivine is that only ejecta from the first, shallower-digging impact reached the Earth. If so, then olivine-rich deeper rocks excavated during the second impact should still be prominently visible among the vestoids. This is definitely not the case, as all of them have

[1]EPSL, Institute of Condensed Matter Physics, Ecole Polytechnique Fédérale de Lausanne (EPFL), Station 3, CH-1015 Lausanne, Switzerland. [2]Physics Institute, Space Research and Planetary Sciences, Center for Space and Habitability, University of Bern, Sidlerstrasse 5, 3012 Bern, Switzerland. [3]Université de Bretagne Occidentale, Institut Universitaire Européen de la Mer, CNRS UMR 6538, Place Nicolas Copernic, 29280 Plouzané, France. [4]School of Earth and Space Exploration, Arizona State University, PO Box 876004, Tempe, Arizona 85287, USA.

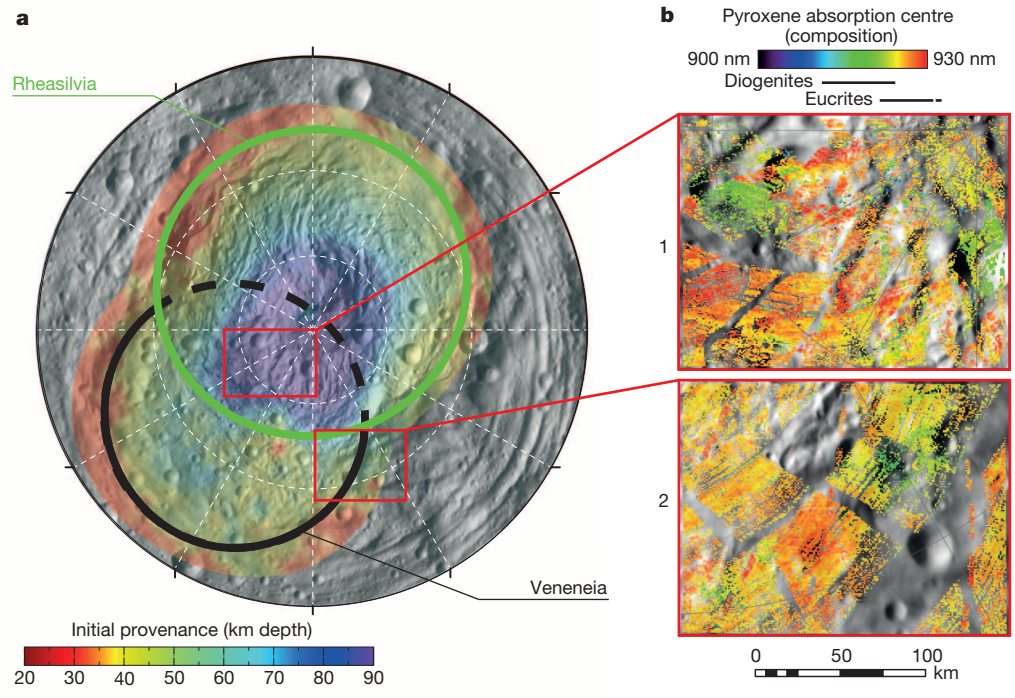

Figure 1 | Pyroxenes composition in regions expected to expose mantle rocks. **a**, Initial provenance (depth) of the exposed material on the surface (from numerical simulations[2]). The rims of the impact basins Rheasilvia and Veneneia are outlined. **b**, Absorption centres from modified Gaussian modelling[28], showing the composition of the pyroxenes. The colours in the two maps in **b** give the absorption centres calculated from MGM for each pixel (results fall between 900 nm and 930 nm). The relation between absorption centres and composition is given by the diogenite and eucrite ranges below the coloured scale (following ref. 9). Eucrites have absorption centres shifted more towards 930 nm than diogenites do and thus cyan and green pixels correspond to diogenites while yellow/orange/red pixels correspond to eucrites. Region 1 (upper red box in **a**), within the two basins and encompassing a portion of Rheasilvia's central peak, is where rocks come from the deepest levels in simulations. Region 2 (lower red box in **a**) shows a diogenite-like lithology[9], suggested to be a major constituent of the uppermost mantle[11]. As in previously published results[9,25], an olivine content higher than the detection threshold is detected nowhere, indicating that no mantle rocks are outcropping.

spectral signatures similar to eucrites, diogenites or a mixture of both[18–20]. Once again, those observations are at odds with the idea of an approximately 30–40-km-thick crust.

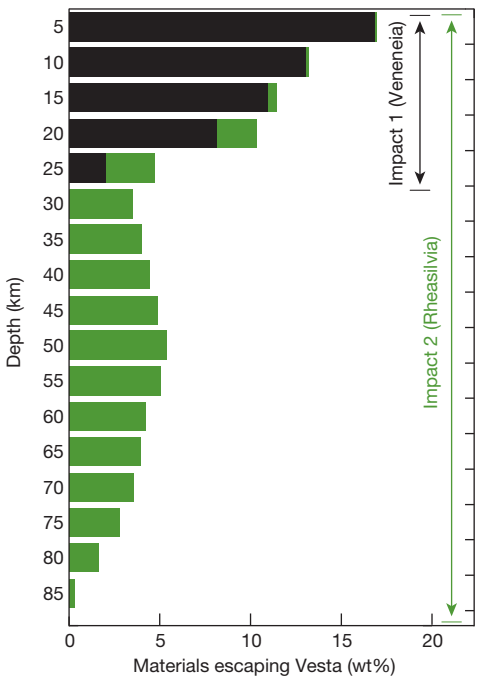

The lack of olivine detections in the Veneneia/Rheasilvia region, and the simultaneous lack of mantle samples among the vestoids/HEDs, together provide evidence that the Moho was not reached during the two impacts. Consequently, the crust of Vesta must be much thicker than 40 km, and possibly as thick as 80 km, according to the cratering simulations. While this is in agreement with the interpretation of gravity data[21], magma-ocean crystallization models are unable to reproduce such a thick crust[7,8]. Indeed, models are required to explain both the oxygen isotopic homogeneity of Vesta and the trace-element features of diogenites[22].

The homogeneity of oxygen isotopic signatures in HEDs attests to a global-scale melting event following accretion[22]. It has been suggested that the deep cumulates formed during the cooling of the magma ocean suffered extensive remelting. The resulting melts could have formed diogenitic intrusions within the massive eucritic crust[23,24] (Fig. 3). The probability of the existence of such crustal intrusions is strengthened by the recent discovery of scattered patches of olivine-rich rocks (50%–80% olivine), hundreds of metres in size, that occur over an area of about a hundred kilometres square in the northern hemisphere of Vesta[25]. As those outcrops are found around impact craters too small to reach the mantle, they might indicate the exhumation of upper crustal plutons, with locally olivine-enriched layers, rather than exposures of a global olivine-rich layer.

Figure 2 | Initial depths and mass fractions of rocks that escaped Vesta. Escaped rocks provides a unique sampling profile of the interior of Vesta. They should be statistically represented in the HED meteorites suite. The relative proportion of material that escaped Vesta, compared to the total mass loss, is given as a function of its original depth before the impacts. Mass fractions and depths are obtained using previously published three-dimensional numerical simulation of impacts[2]. The first impact (Veneneia, in black) ejected mostly material from shallow depths (<25 km) while the second one (Rheasilvia, in green) ejected material from greater depths (mainly between 20 km and 80 km).

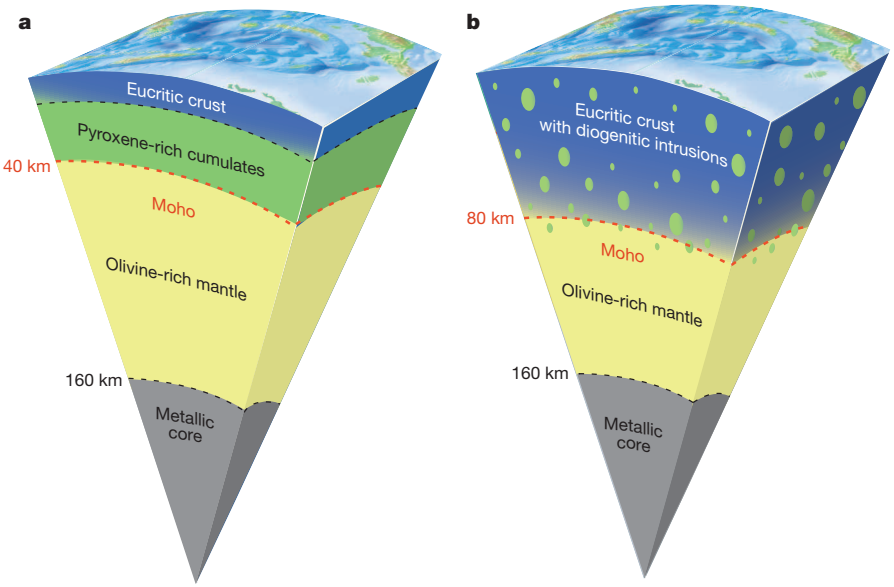

Figure 3 | Potential internal structures for Vesta. **a**, Classical model of the internal layering of Vesta resulting from the crystallization of a magma ocean, generally assuming the crust to be around 40 km thick[7]. **b**, The scenario of eucritic crust intruded by plutons, which leads to a much thicker crust[24]. Diogenetic plutons can have locally olivine-enriched layers. The depth of the core is 160 km (ref. 29).

It has been known since the 1970s that eucrites are poor in sodium and other volatile elements[26]. This might imply that Vesta formed from volatile-poor dusts in an incompletely condensed solar nebula[27], or via a complex path related to inefficient accretion. With a deep Moho, it appears clear that the mantle is much thinner than expected (Fig. 3), leading to the conclusion that Vesta contains far less olivine than predicted by chondritic models[8]. This could be additional evidence that its bulk chemical composition deviates substantially from a chondritic composition for major elements as well.

METHODS SUMMARY

We here analyse data presented in previous papers[2,9]. We use the results of recent three-dimensional SPH modelling[2] to track the dynamical evolution and redistribution of the material during the simulations. Using the initial location of each particle before the impacts, we define the initial depth as the radial distance to the surface and we calculate the provenance of the material that is finally excavated onto the surface or lost from the asteroid (that is, that reach a speed higher than the escaped velocity).

We also analyse data acquired in the southern hemisphere of Vesta by the Dawn VIR instrument. All available images were first processed following previously published pipelines[9,10], which include ISIS3 (http://isis.astrogeology.usgs.gov/) and in-house procedures to correct for photometry, bad pixels and spatial misalignment. We thus produce a global mosaic with a resolution of ten pixels per degree. We then used a recent approach based on the Modified Gaussian Model (MGM)[28] to detect low olivine content in mixtures with pyroxene.

Before any systematic mapping, we additionally tested the capability of the chosen approach to detect large amounts of olivine in HEDs. On the two olivine-diogenites tested (with contents of, respectively, 50% and 57% of olivine), an olivine/pyroxene mixture was successfully detected. A certified limit of about 50% is enough to definitely spot any mantle outcrop (60%–80% olivine) on Vesta's surface, and yet our analyses of VIR data reproduce previous findings where pyroxenes are ubiquitous in the southern hemisphere, but no olivine is observed[9–11].

Online Content Methods, along with any additional Extended Data display items and Source Data, are available in the online version of the paper; references unique to these sections appear only in the online paper.

Received 18 February; accepted 16 April 2014.

1. Schenk, P. *et al.* The geologically recent giant impact basins at Vesta's south pole. *Science* **336,** 694–697 (2012).
2. Jutzi, M., Asphaug, E., Gillet, P., Barrat, J.-A. & Benz, W. The structure of the asteroid 4 Vesta as revealed by models of planet-scale collisions. *Nature* **494,** 207–210 (2013).
3. Ivanov, B. A. & Melosh, H. J. 2D numerical modeling of the Rheasilvia impact formation. *J. Geophys. Res. Planets* **118,** 1545–1557 (2013).
4. McCord, T. B., Adams, J. B. & Johnson, T. V. Asteroid Vesta: spectral reflectivity and compositional implications. *Science* **168,** 1445–1447 (1970).
5. Ruzicka, A., Snyder, G. A. & Taylor, L. A. Vesta as the howardite, eucrite and diogenite parent body: implications for the size of a core and for large-scale differentiation. *Meteorit. Planet. Sci.* **32,** 825–840 (1997).
6. Righter, K. & Drake, M. J. A magma ocean on Vesta: core formation and petrogenesis of eucrites and diogenites. *Meteorit. Planet. Sci.* **32,** 929–944 (1997).
7. Mandler, B. E. & Elkins-Tanton, L. T. The origin of eucrites, diogenites, and olivine diogenites: magma ocean crystallization and shallow magma chamber processes on Vesta. *Meteorit. Planet. Sci.* **48,** 1–17 http://dx.doi.org/10.1111/maps.12135 (2013).
8. Toplis, M. J. *et al.* Chondritic models of 4 Vesta: implications for geochemical and geophysical properties. *Meteorit. Planet. Sci.* **16,** 1–16 (2013).
9. Ammannito, E. *et al.* Vestan lithologies mapped by the visual and infrared spectrometer on Dawn. *Meteorit. Planet. Sci.* **48,** 1–14 http://dx.doi.org/10.1111/maps.12192 (2013).
10. De Sanctis, M. C. *et al.* Spectroscopic characterization of mineralogy and its diversity across Vesta. *Science* **336,** 697–700 (2012).
11. McSween, H. Y. *et al.* Composition of the Rheasilvia basin, a window into Vesta's interior. *J. Geophys. Res.* **118,** 1–12 (2013).
12. Beck, A. W. *et al.* Challenges in detecting olivine on the surface of 4 Vesta. *Meteorit. Planet. Sci.* **48,** 1–11 http://dx.doi.org/10.1111/maps.12160 (2013).
13. McSween, H. Y. *et al.* Dawn; the Vesta-HED connection; and the geologic context for eucrites, diogenites, and howardites. *Meteorit. Planet. Sci.* **48,** 2090–2104 (2013).
14. Binzel, R. P. & Xu, S. Chips off of asteroid 4 Vesta: evidence for the parent body of basaltic achondrite meteorites. *Science* **260,** 186–191 (1993).
15. Bus, S. J. Evidence for spectral color variation within the Vesta family. In *8th Workshop on 'Catastrophic Disruption in the Solar System'* http://www.cd8.hawaii-conference.com/wp-content/uploads/2013/06/CD8_abs_Bus.pdf (2013).
16. Nesvorný, D. *et al.* Fugitives from the Vesta family. *Icarus* **193,** 85–95 (2008).
17. Beck, A. W. & McSween, H. Y. Diogenites as polymict breccias composed of orthopyroxenite and harzburgite. *Meteorit. Planet. Sci.* **45,** 850–872 (2010).
18. Mayne, R. G., Sunshine, J. M., McSween Jr, H. Y., Bus, S. J. & McCoy, T. J. The origin of Vesta's crust: insights from spectroscopy of the Vestoids. *Icarus* **214,** 147–160 (2011).
19. Reddy, V., Nathues, A. & Gaffey, M. J. First fragment of asteroid 4 Vesta's mantle detected. *Icarus* **212,** 175–179 (2011).
20. Buratti, B. J. *et al.* Vesta, vestoids, and the HED meteorites: interconnections and differences based on Dawn Framing Camera observations. *J. Geophys. Res.* **118,** 1991–2003 (2013).
21. Park, R. S. *et al.* Gravity field expansion in ellipsoidal harmonic and polyhedral internal representations applied to Vesta. *Icarus* http://dx.doi.org/10.1016/j.icarus.2013.12.005 (in the press).
22. Greenwood, R. C. *et al.* The oxygen isotope composition of diogenites: evidence for early global melting on a single, compositionally diverse, HED parent body. *Earth Planet. Sci. Lett.* **390,** 165–174 (2014).
23. Barrat, J.-A., Yamaguchi, A., Zanda, B., Bollinger, C. & Bohn, M. Relative chronology of crust formation on asteroid Vesta: insights from the geochemistry of diogenites. *Geochim. Cosmochim. Acta* **74,** 6218–6231 (2010).
24. Yamaguchi, A., Barrat, J.-A., Ito, M. & Bohn, M. Posteucritic magmatism on Vesta: evidence from the petrology and thermal history of diogenites. *J. Geophys. Res.* **116,** E08009 (2011).

25. Ammannito, E. *et al.* Olivine in an unexpected location on Vesta's surface. *Nature* **504,** 122–125 (2013).
26. Tera, F., Eugster, O., Burnett, D. S. & Wasserburg, G. J. Comparative study of Li, Na, K, Rb, Cs, Ca, Sr and Ba abundances in achondrites and in Apollo 11 lunar samples. *Proc. Apollo 11 Lunar Sci. Conf.* **2,** 1637–1657 (1970).
27. Hans, U., Kleine, T. & Bourdon, B. Rb–Sr chronology of volatile depletion in differentiated protoplanets: BABI, ADOR and ALL revisited. *Earth Planet. Sci. Lett.* **374,** 204–214 (2013).
28. Clénet, H. *et al.* A new systematic approach using the Modified Gaussian Model: insight for the characterization of chemical composition of olivines, pyroxenes and olivine–pyroxene mixtures. *Icarus* **213,** 404–422 (2011).
29. Russell, C. T. *et al.* Dawn at Vesta: testing the protoplanetary paradigm. *Science* **336,** 684–686 (2012).

Acknowledgements M.J. acknowledges support from the Swiss National Science Foundation through the Ambizione program. J.-A.B. acknowledges support from the INSU Programme National de Planétologie. E.I.A. was sponsored by the NASA Planetary Geology and Geophysics Program.

Author Contributions H.C. analysed data and led the research. M.J. performed the numerical simulations. P.G. initiated the collaboration and funded part of the research. All authors interpreted the results and contributed to the preparation of the manuscript.

Author Information Reprints and permissions information is available at www.nature.com/reprints. The authors declare no competing financial interests. Readers are welcome to comment on the online version of the paper. Correspondence and requests for materials should be addressed to H.C. (harold.clenet@epfl.ch).

METHODS

Numerical simulations of impact. We here use the results of previously published three-dimensional SPH simulations[2]. In the three-dimensional modelling of the two subsequent impacts, the dynamical evolution and redistribution of the material (SPH particles) was tracked during the simulation. Note that self-gravity was computed throughout the whole simulation. The provenance of surface material shown in Fig. 1 (left) is computed in the same way as in ref. 2. However, here we use a stereographic projection, which corresponds to the same projection as the underlying background.

Using the initial location (before the impacts) of each SPH particle we define the initial depth as the radial distance to the surface of the initially spherical target. To determine whether or not a particle will escape Vesta owing to an impact, we compare its ejection velocity v_{esc} with the escape speed of Vesta, using $v_{esc} = 360\ m\ s^{-1}$. The total mass of ejecta originating from a certain layer of the target is then given by the summation of all particles located within this layer, which have ejection velocities $v_{eject} > v_{esc}$. This procedure is used to analyse both the Veneneia and the Rheasiliva impacts. It can be noted that an increase of the required escape speed leads to a global decrease of the total amount of material escaping Vesta, without, however, affecting the relative distribution among the initial depths.

Although the simulations reproduce well the observed topography of Vesta[2], different initial conditions might lead to a good match as well. The uncertainties are due to the pre-impact shape, the impact angle and velocity of each impact and Vesta's rotation axis, which are all unknown. However, the overall results of our analysis (the provenance of ejecta from deep layers) are expected to be robust since they are mainly produced by the significant overlap of the two giant basins. Moreover, the SPH modelling results are roughly consistent with the findings of ref. 3 when the subsequent formation of both basins is considered.

Processing of Dawn VIR data. We process all the available Dawn VIR[30] images over the southern hemisphere from the High Altitude Mapping Orbit (HAMO) 1 and 2 and from the Low Altitude Mapping Orbit (LAMO) to produce a mosaic similar to the ones published in refs 9 and 10. Images were downloaded from NASA's Planetary Data System Small Bodies Node (http://pds-smallbodies.astro.umd.edu/) with level 1B calibration. They were first processed through the classical ISIS3 pipeline[31] (details for each function can be found in the online ISIS3 manual available at http://isis.astrogeology.usgs.gov/Application/index.html). Each data cube is read with the *dawnvir2isis* procedure. Ground positions and photometric viewing angles are computed using the *spiceinit* function. In parallel, the associated quality and geometry cubes are produced using the *pds2isis* and *phocube* functions respectively. Then pixels where observation angles are too high ($>75^{\circ}$) are removed using *photrim*. Finally, we apply a photometric correction with the *photomet* function (in HapkeHen mode) and using the parameters found in the literature[32–34] (macroscopic roughness parameter $\theta = 20$, single-scattering albedo Wh = 0.52, single-term Henyey–Greenstein coefficient Hg1 = −0.29, width of the opposition surge Hh = 0.04, amplitude of the opposition surge B0 = 1.03).

We then use in-house routines for additional processing. We first filter the bad pixels in each image using the associated quality cube. Because the visible and near-infrared parts of an image are acquired with two distinct detectors[30], geographical misalignments could exist and must be taken into account before the fusion of the two spectral domains. To correct this geographical misalignment, we use the method of the Dawn team[9]. We compute for each detector the latitude/longitude coordinates of the pixels in the corners of the image and we apply, if needed, a simple translation on the visible part to match the infrared coordinates. Images with non-homogenous misalignment are removed from the final mosaic. The conversion from radiance to the irradiance/solar flux is done using Kurucz solar irradiance spectrum resampled at VIR-infrared sampling and resolution. Finally, all the VIR images are projected using the geometry information and assembled in a mosaic (resolution of ten pixels per degree) covering all of the southern hemisphere of Vesta.

The quantitative interpretation of mineralogy from spectra is limited as it is hampered by the overlap of the absorption features, particularly when there is a mixture of two or three minerals[35–37]. The Modified Gaussian Model (MGM)[38–40] aims at deconvolving overlapping absorptions of mafic mineral spectra into their fundamental absorption components. It is achieved by considering a sum of modified Gaussian functions characterized by their band centres, widths and strengths. The specific aim of this model is to account directly for electronic transition processes[38].

However, MGM results are sensitive to the initial parameters[28] and thus it cannot be implemented blindly on an entire data set as acquired on Vesta's surface. An automatic procedure has been implemented to deal with unknown mafic mineralogy in the case of natural rock spectra[28]. An automatic analysis of the shape of the spectrum is first performed (spectrum maxima and minima are used to estimate, to first order, the absorption strengths and widths). The continuum is handled with a second-order polynomial initially adjusted on the local maxima along the spectrum (curvature, slope and shift are free to move during the modelling). All the mixture possibilities involving orthopyroxene, clinopyroxene and olivine are considered[28] and, accordingly, different numbers of Gaussians (from 3 to 7), depending on the potential complexity of the mixture, are used for each of the seven configurations. Additional Gaussians centred around 0.5 μm (ultraviolet charge-transfer absorption), 0.6 μm (ferric absorption) and at 1.4 μm, 1.9 μm and 2.3 μm (hydration and alteration effects) may be requested to account for spectral features not related to mafic mineralogy. The initial settings for the three parameters for each Gaussian for the seven different configurations are made each time on the basis of the spectrum shape and the laboratory results available in the literature in the case of simple mixtures of mafic minerals[28].

Considering all the mixture possibilities with the three mafic components, MGM modelling is run seven times, with seven different initializations, on a given pixel. Root-mean-square residuals cannot be used as the only parameter to check for the validity of the results because a large number of Gaussian functions may result in low root-mean-square mathematical solutions without any physical meaning. Consequently, the returned MGM solutions are then assessed on the basis of a mineralogical sorting (that is, each modelled Gaussian functions must verify the spectroscopic criteria defined in the literature[35,39,40]) and are accordingly either validated or discarded. Finally, the solutions kept are interpreted in terms of mineralogy[28].

The uncertainties on the calculated band centres have been determined on laboratory spectra to be ±8 nm in the 1-μm domain (and ±17 nm in the 2-μm domain, which is not used here)[41]. Those uncertainties are relevant because the absorption depths in the VIR data are comparable to the depths observed in the laboratory[33].

The adapted MGM approach is able to model both simple and complex mafic mineralogies, including binary and ternary mixtures (involving orthopyroxene, spectral type B clinopyroxene and olivine) for a large range of grain sizes. It has been extensively validated on a large range of laboratory spectra, in particular on some that are representative of HED compositions (various olivine-orthopyroxene mixtures with similar chemistry)[28]. It was originally shown to be able to detect an olivine content as low as 10% to 50% on laboratory spectra[28], the exact limit depending mainly on the chemical composition and the grain size of each minerals in the mixture. The adapted MGM approach has also been validated in natural conditions on Earth[42], the Moon[43] and Mars[44], each time allowing the detection of olivine with or without pyroxenes.

Nevertheless, before any systematic mapping on Vesta's surface, we choose to test the capability of this approach to detect significant amount of olivine on HEDs. We use two spectra from the meteorites NWA4223 and NWA5480 (ref. 45). Both are olivine-diogenites with olivine contents of 50% and 57%, respectively. We note that both spectra also show effects of terrestrial weathering, which can affect the spectral slope. Nevertheless, the continuum allows us to take into account this effect in the MGM approach and Earth validation has shown that band centre results remain reliable[42].

The spectra clearly exhibit strong pyroxene signatures (Extended Data Fig. 1); however, in both cases MGM results confirm the detection of an olivine/pyroxene mixture, thus verifying the ability of the approach to detect systematically contents of at least 50% olivine. Magma-ocean crystallization models and simple mass-balance and thermodynamic constraints agree on the harzburgitic nature (>40% olivine mixed with orthopyroxene) of Vesta's mantle[7,8]. The predicted olivine content lies within the range 60%–80%, which differs significantly from the low olivine abundances observed in the lithologies from the pyroxene-rich crust (olivine-diogenites generally contain less than 30% of olivine[12,17]). Therefore, a certified limit of ~50% is enough to definitely spot any mantle outcrop (60%–80% olivine) on Vesta's surface.

30. De Sanctis, M. C. *et al.* The VIR spectrometer. *Space Sci. Rev.* **163,** 329–369 (2011).
31. Anderson, J. *et al.* Isis cartographic tools for the Dawn Framing Camera and Visual and Infrared Spectrometer. *AGU Fall Meet.* Abstr. U31A–0009 (American Geophysical Union, 2011).
32. Reddy, V. *et al.* Color and albedo heterogeneity of Vesta from Dawn. *Science* **336,** 700–704 (2012).
33. De Sanctis, M. C. *et al.* Vesta's mineralogical composition as revealed by the visible and infrared spectrometer on Dawn. *Meteorit. Planet. Sci.* **48,** 1–19 http://dx.doi.org/10.1111/maps.12138 (2013).
34. Li, J.-Y. *et al.* Photometric properties of Vesta. In *Asteroids, Comets, Meteors Conf.* (eds Li, J.-Y. *et al.*) abstr. 6387 (2012).
35. Adams, J. B. Visible and near IR diffuse reflectance spectra of pyroxenes as applied to remote sensing of solid objects in the solar system. *J. Geophys. Res.* **79,** 4829–4836 (1974).
36. Singer, R. B. Near-infrared spectral reflectance of mineral mixtures: systematic combinations of pyroxenes, olivine and iron oxides. *J. Geophys. Res.* **86,** 7967–7982 (1981).
37. Cloutis, E. A. & Gaffey, M. J. Spectral-compositional variations in the constituent minerals of mafic and ultramafic assemblages and remote sensing implications. *Earth Moon Planets* **53,** 11–53 (1991).
38. Sunshine, J. M., Pieters, C. M. & Pratt, S. F. Deconvolution of mineral absorption bands: an improved approach. *J. Geophys. Res.* **95,** 6955–6966 (1990).

39. Sunshine, J. M. & Pieters, C. M. Estimating modal abundances from the spectra of natural and laboratory pyroxene mixtures using the modified Gaussian model. *J. Geophys. Res.* **98,** 9075–9087 (1993).
40. Sunshine, J. M. & Pieters, C. M. Determining the composition of olivine from reflectance spectroscopy. *J. Geophys. Res.* **103,** 13675–13688 (1998).
41. Kanner, L. C., Mustard, J. F. & Gendrin, A. Assessing the limits of the Modified Gaussian Model for remote spectroscopic studies of pyroxenes on Mars. *Icarus* **187,** 442–456 (2007).
42. Clenet, H. Télédétection hyperspectrale: minéralogie et pétrologie, application au volcan Syrtis Major (Mars) et à l'ophiolite d'Oman. PhD thesis, Univ. Toulouse, http://thesesups.ups-tlse.fr/501/ (2009).
43. Clenet, H., Isaacson, P. J. & Gillet, P. Systematic mapping of mafic minerals in the Copernicus region, the Moon: an improved approach based on Modified Gaussian Model applied to M3 data. *Lunar Planet. Sci. Conf.* **1822** (2014).
44. Clenet, H. *et al.* A systematic mapping procedure based on the Modified Gaussian Model to characterize magmatic units from olivine/pyroxenes mixtures: application to the Syrtis Major volcanic shield on Mars. *J. Geophys. Res.* **118,** 1632–1655 (2013).
45. Beck, P. *et al.* NIR spectral trends of HED meteorites: can we discriminate between the magmatic evolution, mechanical mixing and observation geometry effects? *Icarus* **216,** 560–571 (2011).

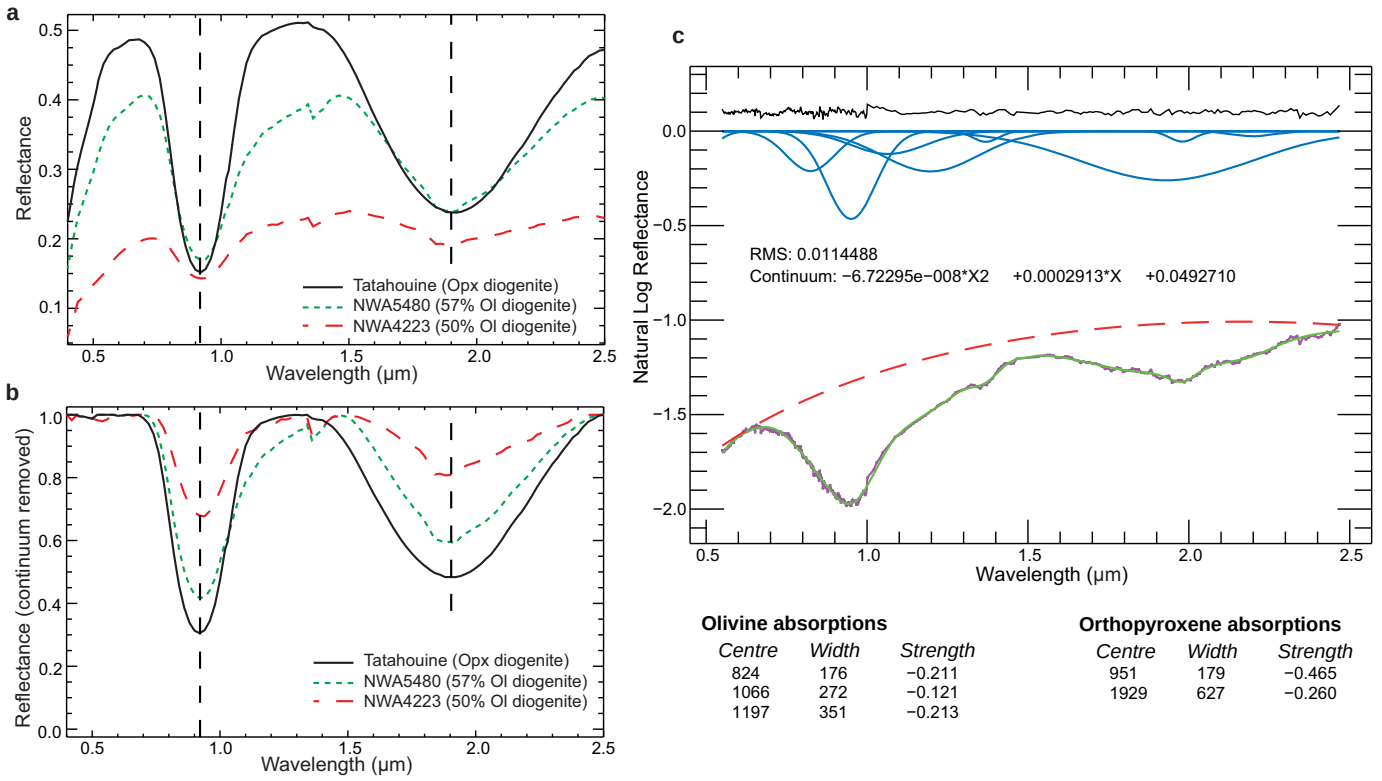

Extended Data Figure 1 | Olivine-diogenite spectra and MGM result for NWA4223. Olivine–diogenite spectra from meteorites NWA5480 and NWA4223 (57% and 50% olivine respectively) and comparison with a spectrum from diogenite Tatahouine (orthopyroxenite). Spectra are represented in reflectance space (**a**) and with the continuum removed (**b**) for visual comparison of the shape of the absorption. The MGM result for the NWA4223 spectrum is represented in **c**. The parameters (from left to right the centre, width and strength are shown) for each Gaussian function (three for olivine and two for orthopyroxene), the continuum and the residual (root mean square, RMS) are reported. Olivine and pyroxene are both correctly detected. Opx, orthopyroxene; Ol, olivine.